inorganics

MDPI

Article

Methacrylic Photopolymerizable Resin Incorporating Selenium Nanoparticles as a Basis for Additive Manufacturing of Functional Materials with Unique Biological Properties

Dmitriy E. Burmistrov [1], Ilya V. Baimler [1], Fatikh M. Yanbaev [2], Maxim E. Astashev [1], Valeriy A. Kozlov [1,3], Dmitry A. Serov [1], Aleksandr V. Simakin [1] and Sergey V. Gudkov [1,*]

[1] Prokhorov General Physics Institute of the Russian Academy of Sciences, Vavilov Str. 38, 119991 Moscow, Russia; dmitriiburmistroff@gmail.com (D.E.B.); ilyabaymler@yandex.ru (I.V.B.); astashev@yandex.ru (M.E.A.); v.kozlov@hotmail.com (V.A.K.); dmitriy_serov_91@mail.ru (D.A.S.); avsimakin@gmail.com (A.V.S.)
[2] Federal Research Center Kazan Scientific Center of the Russian Academy of Sciences, ul. Lobachevskogo 2/31, Tatarstan, 420088 Kazan, Russia; f.yanbayev@knc.ru
[3] Department of Fundamental Sciences, Bauman Moscow State Technical University, 52nd Baumanskaya St., 105005 Moscow, Russia
* Correspondence: s_makariy@rambler.ru

Abstract

Despite the widespread use of photopolymerizable methacrylate resins in additive manufacturing, their potential for creating functional biomedical materials remains untapped. Standard resins, while possessing good technological properties, are typically biologically inert and unable to combat such a critical problem as bacterial colonization. In this work, we propose incorporating selenium nanoparticles (Se NPs) into a photopolymerizable resin based on methacrylate monomers to obtain functional composite materials in the MSLA printing process. Composite material samples made from modified resins showed no structural surface defects and were characterized by a non-uniform distribution of NPs in volume and demonstrated a higher degree of monomer conversion. The materials demonstrated significant antioxidant activity, removing OH-radicals and H_2O_2 and reducing the level of biomarkers of oxidative damage (8-oxoguanine in DNA and long-lived reactive protein species). A dose-dependent bacteriostatic effect was observed in *E. coli* cell cultures against a background of high cytocompatibility with human cell cultures. The developed photopolymerizable resins modified with Se NPs allow obtaining products that combine the properties of a bacteriostatic agent with antioxidant properties and high biocompatibility, which is of considerable interest in terms of materials for biomedical applications.

Keywords: methacrylic photopolymerizable resin; selenium nanoparticles; bacteriostatic; ROS; cytocompatibility

check for updates

Academic Editor: Eduardo Padilla-Camberos

Received: 29 September 2025
Revised: 28 October 2025
Accepted: 30 October 2025
Published: 1 November 2025

Citation: Burmistrov, D.E.; Baimler, I.V.; Yanbaev, F.M.; Astashev, M.E.; Kozlov, V.A.; Serov, D.A.; Simakin, A.V.; Gudkov, S.V. Methacrylic Photopolymerizable Resin Incorporating Selenium Nanoparticles as a Basis for Additive Manufacturing of Functional Materials with Unique Biological Properties. *Inorganics* **2025**, *13*, 365. https://doi.org/10.3390/inorganics13110365

Copyright: © 2025 by the authors. Licensee MDPI, Basel, Switzerland. This article is an open access article distributed under the terms and conditions of the Creative Commons Attribution (CC BY) license (https://creativecommons.org/licenses/by/4.0/).

1. Introduction

The current stage of additive manufacturing development is characterized by an active search for new functional materials that combine improved physicochemical characteristics with controlled biological activity [1–3]. With the rapid development of photopolymer printing technology, research aimed at modifying polymer materials derived from methacrylate resins (MRs), which are widely used in various fields of medicine due to their biocompatibility and technological properties, is becoming particularly relevant [4]. A promising approach for enhancing these materials involves the incorporation of nanoscale additives, which have the potential to substantially modify the functional properties of the polymer

matrix [5–8]. Possessing enormous potential in engineering and biomedicine, NPs have also demonstrated efficacy as antibacterial agents. Their multimodal action, aimed at disrupting microbial homeostasis, includes direct interaction with bacterial cell walls, inhibition of biofilm formation, ion release, generation of reactive oxygen species (ROS), and disruption of DNA and protein synthesis [9]. Among the various types of NPs, selenium nanoparticles (Se NPs) are of particular scientific and practical interest [10–12] due to their pronounced antimicrobial activity against a wide range of pathogenic microorganisms, including Gram-positive and Gram-negative bacteria, as well as fungal pathogens [13–15]. The distinctive features of Se NPs that are attractive from the point of view of biomedical properties are their biocompatibility, bioavailability, and low toxicity [16,17]. Selenium, a component of selenoproteins and selenium-containing compounds in the human body, performs critical biological functions, including ensuring DNA replication and synthesis, regulating thyroid hormone synthesis, metabolic processes, and protection against infectious agents and oxidative stress [18–20]. Selenium plays a special role as a biochemical cofactor of glutathione peroxidase, a key antioxidant enzyme responsible for preserving thiol groups and catabolizing peroxides [21]. The bactericidal properties of selenium are associated with its ability to catalyze the oxidation of intracellular thiols, leading to the death of microorganisms [22]. According to current understanding, selenium, being an essential trace element, potentiates the activity of selenium-dependent enzymes, providing protection for cells and tissues from free radical damage in vivo [23]. Selenium, including its nanoform, is widely utilized in the production of food supplements and as a component in agricultural fertilizers [24]. In addition to their biological significance, Se NPs have gained significant industrial and commercial traction due to their distinctive physicochemical properties, including high photoconductivity and low melting point. These properties contribute to their pronounced catalytic activity in organic hydration and oxidation reactions, making them valuable in a variety of industrial and commercial applications [25]. The incorporation of Se NPs into photopolymerizable composites allows the creation of materials with controllable surface properties that provide resistance to bacterial adhesion and biofilm formation [26]. The materials obtained may be of considerable interest for the development of a new generation of products that combine structural integrity with the prevention of bacterial contamination [27]. However, the practical implementation of this approach entails the resolution of several fundamental and applied problems. The primary challenges pertain to the controlled dispersion of NPs within the polymer matrix [28], the attainment of adequate interphase compatibility [29], and the comprehensive evaluation of the biological safety of the resulting compositions [30]. A particular emphasis should be placed on the examination of the impact of nanoparticle integration on the conversion efficiency of methacrylate monomers, given its pivotal role in determining the structural uniformity and performance attributes of the final products [31,32].

In this regard, the aim of this study is to develop a series of new photopolymerizable composites based on methacrylate photopolymerizable resin modified with Se NPs at varying concentrations and to comprehensively study the relationship between the structure, properties, and biological activity of the obtained materials. The objectives of the work include the following: synthesis and characterization of Se NPs, development of a method for their incorporation into photopolymerizable resin, additive manufacturing of finished samples of products from these materials, study of the physicochemical properties of the obtained materials, study of the antimicrobial activity of the obtained samples, as well as study of their in vitro cytocompatibility.

2. Results

According to dynamic light scattering data, the size distribution of NPs in the colloid is unimodal. The majority of particles are approximately 75 nm in size, with the peak width of the distribution being approximately 50 nm (Figure 1a). The distribution of the electrokinetic potential of Se NPs in the colloid was studied (Figure 1b). The presence of a clearly defined maximum in the region of −35 mV in the monomodal distribution of the electrokinetic potential indicates the high stability of the synthesized colloidal solution of NPs. The optical properties of the colloid of NPs were studied (Figure 1c). It was shown that the colloid exhibits moderate absorption in the visible wavelength range of 380–750 nm, characteristic of amorphous selenium (Se^0) NPs, and has a characteristic absorption peak in the region of 260–265 nm. The morphology of Se NPs obtained by laser ablation of a solid selenium target in water was studied using transmission electron microscopy (Figure 1d). The shape of selenium NPs was close to spherical, and their average size was approximately 70 nm.

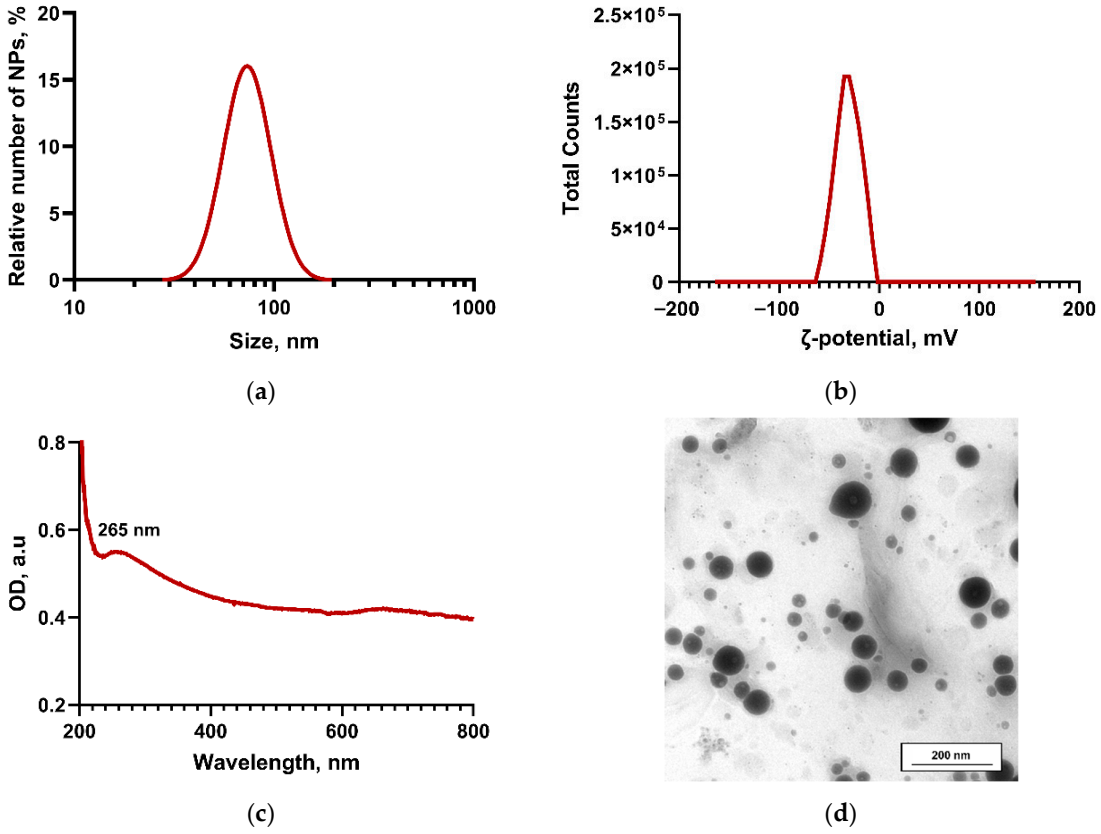
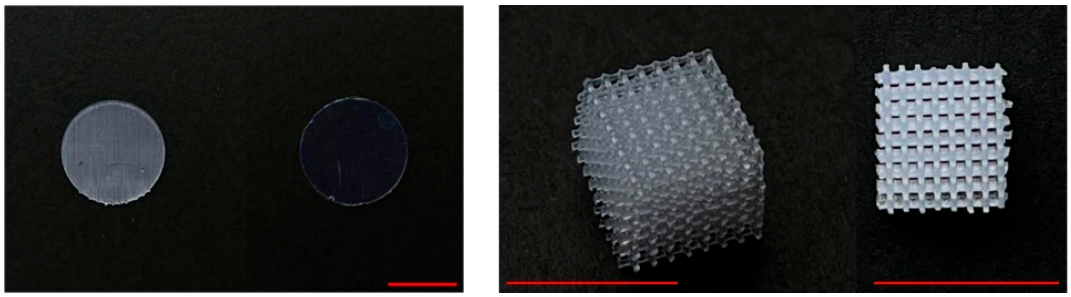


Figure 1. Physical and chemical properties of Se NPs obtained by laser ablation. Size distribution of NPs obtained by dynamic light scattering (**a**). Distribution of the ζ-potential of Se NPs in a colloid (**b**). Absorption spectrum of Se colloid in the UV and visible ranges (**c**). Image of Se NPs obtained using a transmission electron microscope (scale bar 200 nm) (**d**).

Se NPs were added to MR in three different concentrations: 0.001, 0.01, and 0.1 w%. Using MSLA 3D printing, composites from the obtained modified Se NPs-MRs were printed in the form of round plate samples with Ø16 mm and a thickness of 0.5 mm (Figure 2a). The resulting composite samples were ground and polished to evaluate the possibility of mechanical post-processing of the products. During the polishing process, an optically transparent sample was obtained even from MR with a Se NPs content of 0.1 w%. That is, even the resin with the highest content of NPs used in the study can be polished perfectly. To demonstrate the printing accuracy of Se NPs-MRs, a spongy porous sample with a

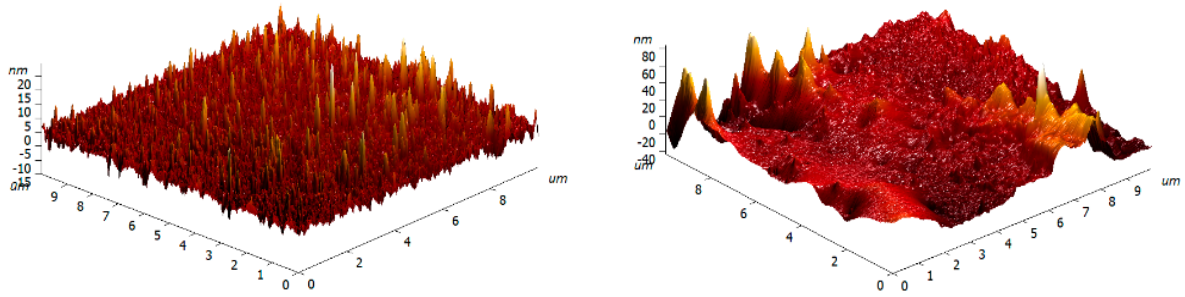
regular structure was made (Figure 2b). It was shown that the edges are continuous throughout the product and have a thickness of about 50 µm even when using MR resin with a Se NPs content of 0.1 w%.



(**a**) (**b**)

Figure 2. Photographs of products made from Se NPs-MR resin with a Se NPs concentration of 0.1 w%. Photographs of printed samples made from modified Se NPs-MR resin, left—before polishing, right—after (**a**); photograph of a volumetric porous sample in two projections (**b**). The scale bar in all photographs corresponds to 10 mm.

To study the surface characteristics of printed composite materials, pre-polished samples in the form of round plates were analyzed using AFM in semi-contact mode (Figure 3a,b). The analysis of the surface topology showed a high degree of uniformity of all samples studied, with no significant structural defects. No cracks, fractures, or cavities were found in any of the samples. Surface roughness was detected in both the control samples and the samples made from composites with NPs. It should be noted that for the surfaces of samples printed from Se NPs-MR, an increase in the profile height was observed, with the presence of protrusions with a height of about 60–80 nm, distributed pseudo-uniformly on the surface.



(**a**) (**b**)

Figure 3. Reconstruction of the surfaces of a polished plate sample printed from MR (**a**) and from Se NPs-MR containing 0.1 w% Se NPs (**b**).

To characterize the hydrophilic-hydrophobic properties of the surfaces of composites obtained from MR with a reduced increase in Se NPs, the method of static contact angle analysis ("sessile drop") was used (Figure 4a–e). The obtained angle values (θc) are shown in Figure 4e. The measurements show that the surface of the samples made from MR without the addition of Se NPs is moderately hydrophilic, as evidenced by the average θc value of approximately 55°. The introduction of Se NPs into the polymer matrix, located to the depth of the study structure, did not reveal statistically significant changes in the contact angle shapes compared to the control sequence. Nevertheless, data analysis revealed a clear trend towards a decrease in θc values with the appearance of a proportion of Se NPs.

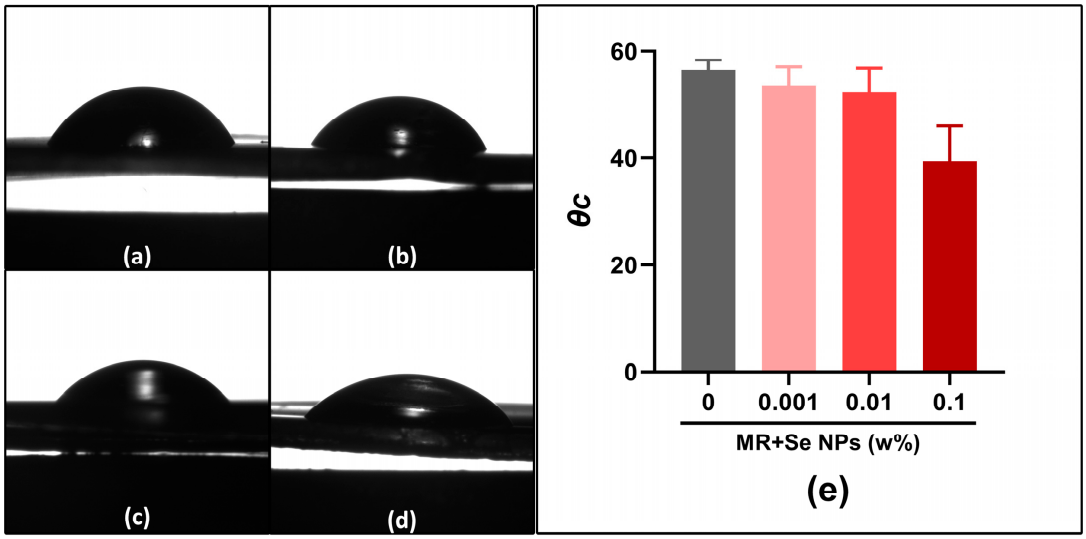
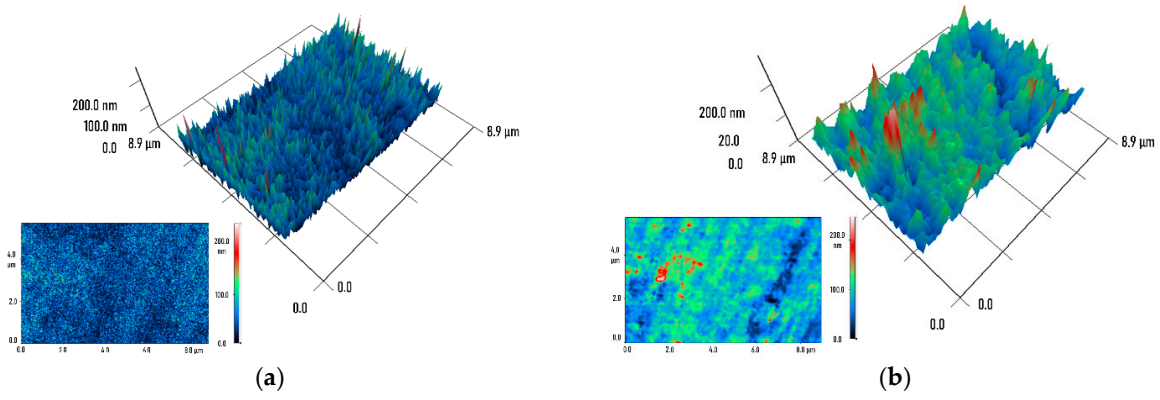


Figure 4. Representative droplet profiles on the surfaces of composites printed from MR without Se (**a**) and composites printed from Se NPs-MR containing Se in concentrations of 0.001% (**b**), 0.01% (**c**), and 0.1% (**d**). Results of contact angle (θc) assessment for material samples (**e**).

The distribution of Se NPs in the volume of composite materials obtained by additive manufacturing from Se NPs-MR was investigated using modulation interference microscopy (MIM). This technique allows the detection of optical inhomogeneities caused by a significant difference in refractive indices between MR (n = 1.49) and elemental selenium Se^0 (n = 3.07). Analysis of the micrographs revealed significant differences between the control and modified samples. The control samples of pure polymer material showed an optically homogeneous structure with no visible inhomogeneities (Figure 5a), indicating the absence of defects during additive manufacturing, such as voids, pores, or inclusions. The introduction of Se NPs led to the appearance of pronounced optical inhomogeneities, the size and density of which showed a direct dependence on the dopant concentration. In the micrographs obtained using MIM, these inhomogeneities are visually represented as areas with warm color tones (Figure 5b–d). In composites with a Se NP content of 0.001%, local inhomogeneities with a size of approximately 0.1 × 0.1 were observed (Figure 5b). An increase in concentration to 0.01% was accompanied by an increase in the size of inhomogeneities to 0.2 × 0.2 µm (Figure 5c). More pronounced structural changes were recorded in samples with 0.1% Se NPs, where extensive areas of optical inhomogeneities ranging from 1–2 µm to 2 µm in diameter and >8 µm in length were identified (Figure 5d).



(**a**) (**b**)

Figure 5. *Cont.*

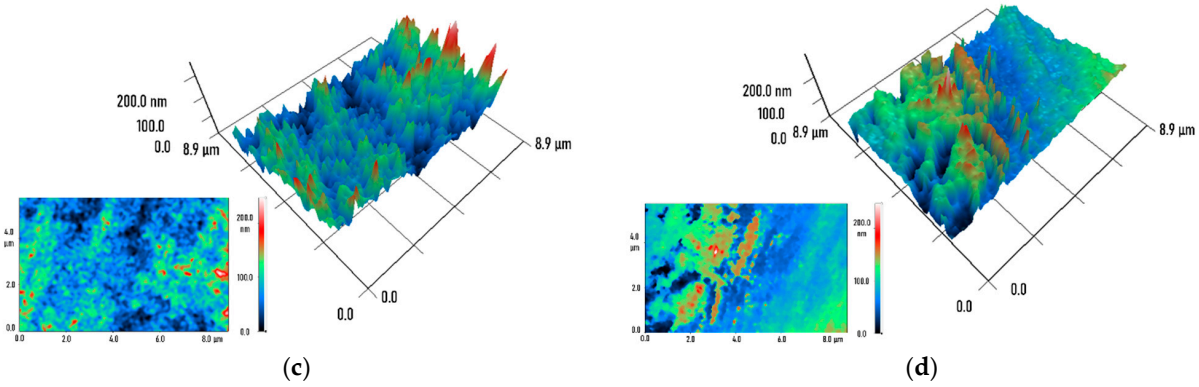


Figure 5. MIM micrographs of composites printed from MR without Se (**a**) and composites printed from Se NPs-MR containing Se in concentrations of 0.001% (**b**), 0.01% (**c**), and 0.1% (**d**). 3D reconstructions of 8.9 × 8.9 µm sections of the materials and the raw data on which they are based (insets at bottom left) are shown. The color represents the phase difference in the transmitted radiation (red—maximum value, blue—minimum).

To investigate the effect of Se NPs on the molecular structure of the polymer matrix, a comprehensive spectral analysis was performed in the infrared, visible, and ultraviolet regions. Average IR Fourier transmission spectra were obtained for a series of composite materials studied. Particular attention was paid to the analysis of characteristic absorption bands in the 1600–1650 cm^{-1} region, corresponding to the valence vibrations of C=C double bonds (Figure 6a). The analysis revealed a significant decrease in the intensity of the characteristic C=C bands in composites containing 0.01 and 0.1 w% Se NPs compared to the control sample of pure polymer. Figure 6b shows the absorption spectra of printed samples of MR and Se NPs-MR in the UV-visible region. Analysis of the spectral characteristics showed that the introduction of Se NPs in the studied concentration range (0.001–0.1 w%) does not lead to significant changes in the optical properties of the polymer matrix in the visible region of the spectrum. All samples retained high optical transparency in the 450–700 nm range, indicating good compatibility of the composite components and the absence of significant light scattering.

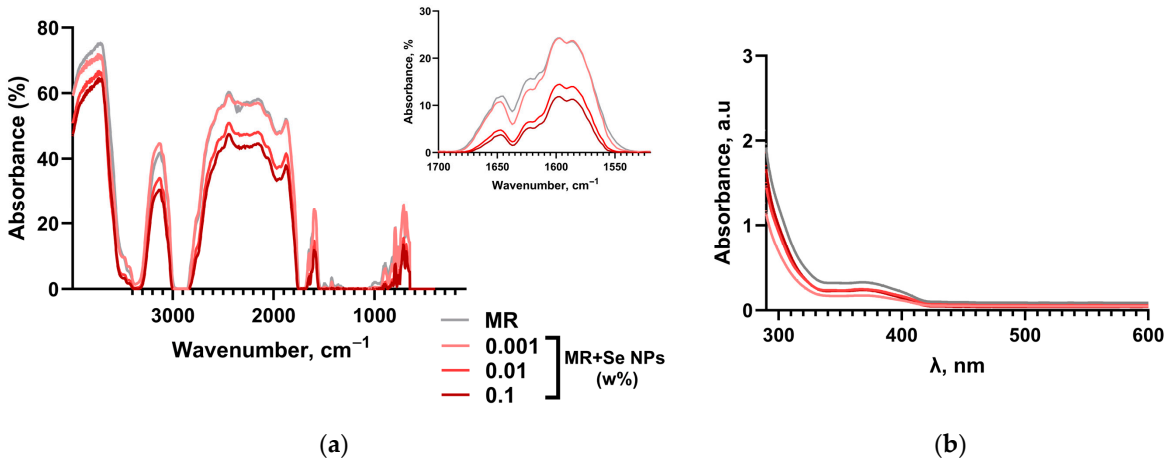


Figure 6. Investigation of the spectral properties of samples printed from MR and Se NPs-MR. IR transmission spectra of composite plate samples printed from Se NPs-MR with different Se NPs contents; inset: enlarged spectral region with lines corresponding to C=C double bonds (**a**). Absorption spectra in the UV/visible range of composite plate samples with different Se NP contents (**b**).

The influence of the obtained composite materials on the generation of reactive oxygen species (ROS), in particular hydrogen peroxide and hydroxyl radicals, in aqueous solutions

was investigated. The experimental results demonstrated a statistically significant increase in the formation of the studied ROS when using polymer samples obtained from MR. In contrast, incubation of aqueous solutions with composite samples printed from Se NPs-MR led to a significant decrease in the concentration of the studied reactive oxygen species. Quantitative determination of hydrogen peroxide showed a decrease in concentration of ~25 and 35% when using composites containing 0.01 and 0.1 w% Se NPs, respectively, compared to pure polymer (Figure 7a); A similar effect was observed for the level of hydroxyl radicals (Figure 7b), where the decrease in concentration was also ~25 and 35% for 0.01 and 0.1 w% Se NPs, respectively. Thus, the most pronounced antioxidant effect of composite materials was observed at the maximum concentration of Se NPs (0.1 w%), at which the level of the studied ROS remained within the control values (~3 nM for H_2O_2 and ~19 nM for ·OH).

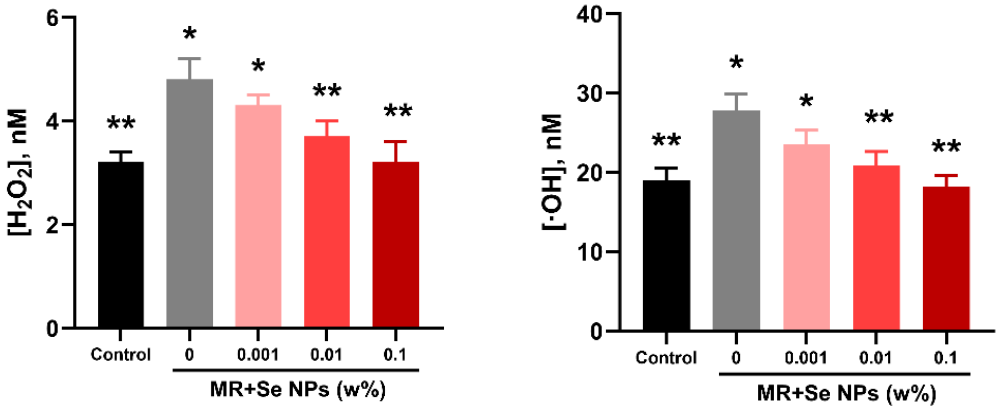


Figure 7. Results of quantitative assessment of hydrogen peroxide (**a**) and hydroxyl radical (**b**) concentrations formed in aqueous solutions after incubation with composite plate samples printed from MR and Se NPs-MR with different Se NP contents (0–0.1 w%). *—difference from control, $p < 0.05$; **—differences relative to polymer samples not containing Se NPs (0 w%), $p < 0.05$.

The effect of composite samples printed from Se NPs-MR on the oxidative modification of DNA and proteins was studied. Using ELISA with antibodies specific to 8-oxoGua, it was found that samples printed from both MR and composites containing 0.001 and 0.01 w% Se NPs did not lead to a significant change in the level of assessed oxidative DNA damage. However, a tendency toward an increase in 8-oxoGua was observed when pure polymer samples were used; while composites impregnated with Se NPs at a concentration of 0.1 w% demonstrated the ability to inhibit the formation of oxidative DNA damage, keeping the level of 8-oxoGua in vitro ~29% lower than that of the pure polymer, which corresponds to the control group (Figure 8a).

The influence of the synthesized composites on the oxidative modification of bovine serum albumin, namely on the formation of LRPS, was studied (Figure 8b). A tendency to induce LRPS formation was observed when protein solutions were incubated with samples printed from MR not containing Se NPs (by ~14% compared to control values). At the same time, all composite samples printed from Se NPs-MR prevented the formation of LRPS. The half-life of LRPS in all groups was 5 h. The differences compared to the control group after 5 h of incubation with material samples were approximately 15, 25, 21, and 6% for samples containing 0, 0.001, 0.01, and 0.1 w% Se NPs, respectively.

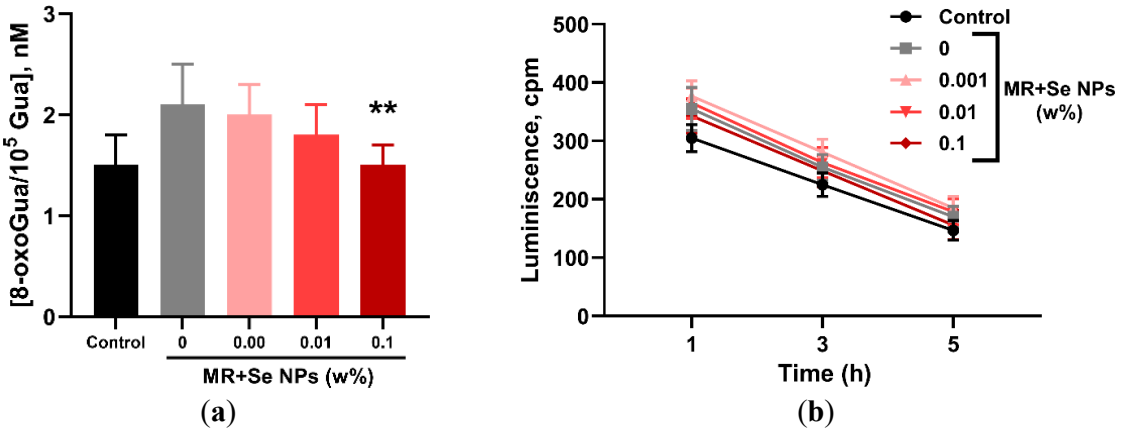


Figure 8. Results of the assessment of the effect of the obtained composite materials on biomolecules in vitro. Effect of composites printed from Se NPs-MR on the concentration of 8-oxoguanines in DNA (**a**) and the level of long-lived reactive protein species (**b**). **—differences relative to polymer samples not containing Se NPs (0 w%), $p < 0.05$.

During a microbiological study of the antibacterial activity of the obtained composite materials against a suspension of *E. coli* cells (Figure 9), the kinetic curves of bacterial culture growth over a 24 h incubation period were analyzed. Samples made from unmodified MR resin did not have a statistically significant effect on the duration of the lag phase, but caused a decrease in the maximum optical density of the bacterial culture by approximately 25% compared to the control. Modification of the MR resin with Se NPs at concentrations of 0.001–0.1% led to a significant suppression of microorganism growth upon contact with the printed samples, which resulted in a decrease in the maximum density of bacterial cultures by 75–85% relative to the control values. Moreover, the time parameters of the lag phase of suspension culture growth in the presence of Se NPs-MR composites did not differ statistically significantly from either the control group or the pure polymer samples (from MR).

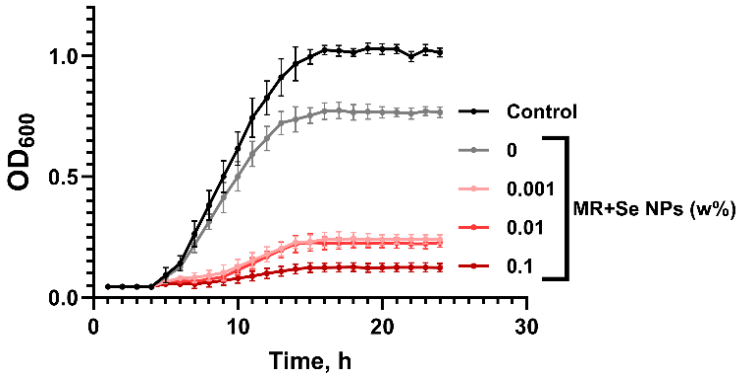


Figure 9. Growth curves of *E. coli* suspension cultures grown in the presence of the tested materials.

Quantitative assessment of the bactericidal activity of the composites using flow cytometry (Figure 10) showed that after 24 h incubation with *E. coli* cultures, neither the pure MR polymer samples nor the Se NPs-MR composite samples with Se nanoparticle content of 0.001 and 0.01 wt.% caused a significant increase in the proportion of dead bacterial cells. A reliable bactericidal effect was observed only when using composites containing 0.1 w% Se NPs, with the proportion of PI-positive cells amounting to about 20% of the total number of bacterial cells in the cultures.

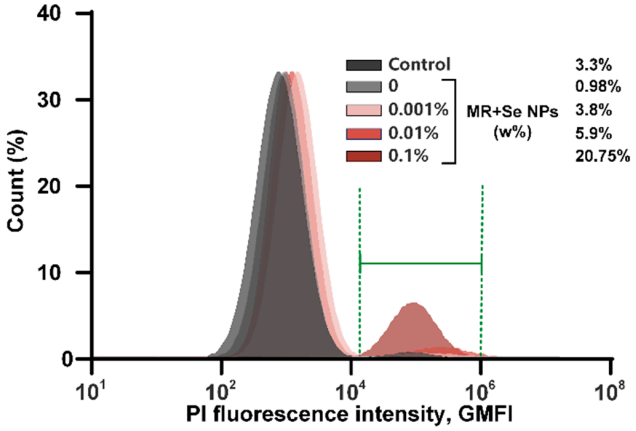


Figure 10. Histograms of bacterial cell distribution by mean geometric PI intensity during incubation with samples of the materials under study. The green interval displays the analyzed gate in the region of the PI-positive cell population.

When bacterial suspensions were incubated with samples printed from MR not containing Se NPs, a statistically significant decrease in the concentration of bacterial cells of ~30% was observed compared to the control group. For samples obtained from Se NPs-MR, a significant dose-dependent inhibition of bacterial growth was observed. The total concentration of *E. coli* cells in the presence of composite samples was lower compared to the control values: a reduction in the concentration of *E. coli* cells by ~80, 85 and 90% was observed for materials containing 0.001, 0.01 and 0.1%, respectively (Figure 11a). At the same time, the bactericidal effect for composite materials was less pronounced and was observed only at the maximum concentration of Se NPs (0.1 w%)—20.75%; while for materials containing 0, 0.001, and 0.01 w% Se NPs, the percentage of PI-positive cells was in the range of 1–6% (Figure 11b).

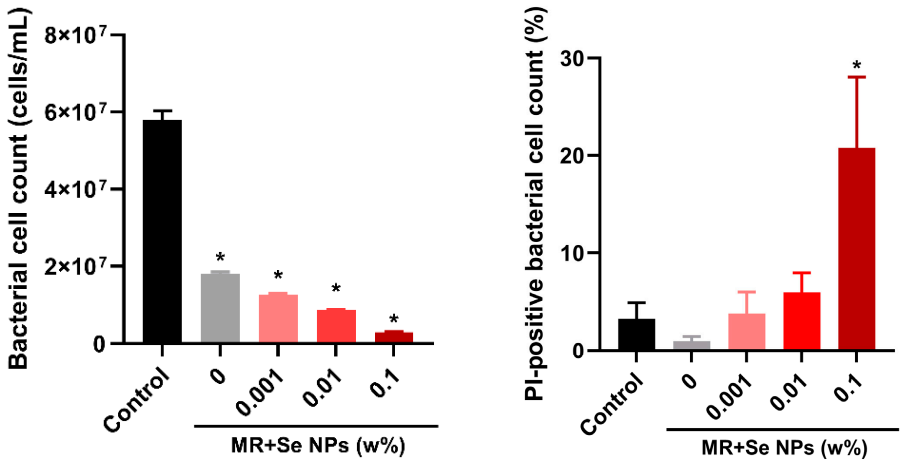


Figure 11. Concentration of *E. coli* bacterial cells (**a**) and proportion of non-viable cells (**b**) after 24 h of cultivation in the presence of composites printed from Se NPs-MR with different Se content (0–0.1 w%). *—difference from control, $p < 0.05$.

A study of the effect of the obtained materials on human skin fibroblast (HSF) cultures showed the absence of significant toxic effects in all samples studied. Microscopic analysis revealed a partial change in the morphology of individually localized cells during prolonged cultivation in the presence of the composite samples under study (Figure 12a–e). Fluorescence microscopy with specific dyes was used for detailed morphological analysis

and assessment of cell viability in cultures. Cell nuclei were visualized using the fluorescent DNA-binding dye Hoechst. Rhodamine 123, a dye that selectively accumulates in the mitochondria of living cells and allows assessment of the total area and shape of cells, was used for contrasting highlighting of the cytoplasmic compartment (Figure 12f). Propidium iodide staining was used to visualize non-viable cells. Quantitative assessment based on differential staining demonstrated a high level of cell viability in all experimental groups studied. The proportion of viable cells consistently ranged from 95% to 100%, indicating the absence of a toxic effect of the experimental conditions used on the cell population (Figure 13a). No significant change in the area of cell nuclei in cultures, compared to the control group, was found in any of the experimental groups; The cell nuclear areas ranged from 270 to 320 μm^2 (Figure 13b). Similarly, the assessment of individual cell areas based on the analysis of rhodamine 123 stained images showed no significant differences between the groups. There was a slight trend toward increased cell area in the cells cultured with Se NPs-containing material samples (Figure 13c,d).

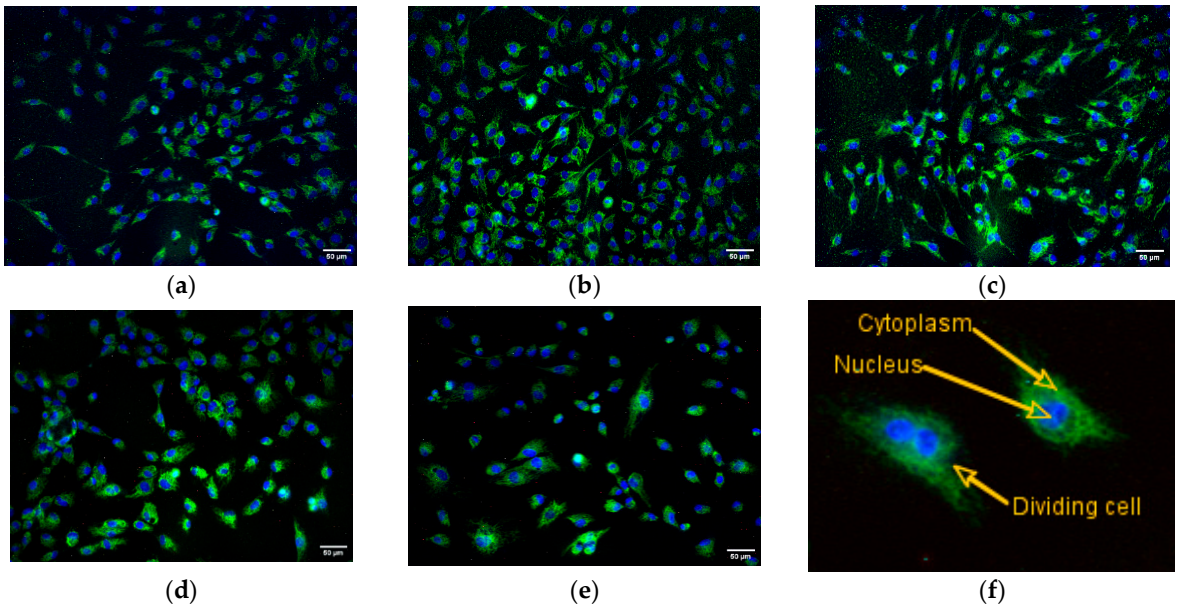


Figure 12. Representative micrographs of HSF cell cultures after 72 h (DIV 3) of cultivation under control conditions (**a**), with samples printed from MR (**b**) and composites from Se NPs-MR with 0.001% (**c**), 0.01% (**d**) and 0.1% (**e**) Se NPs. Merged images of Hoechst 33342 (blue), Rhodamine 123 (green) and PI (red) fluorescence are shown. Photo of individual cells with stained nuclei and contrasted cytoplasm (**f**).

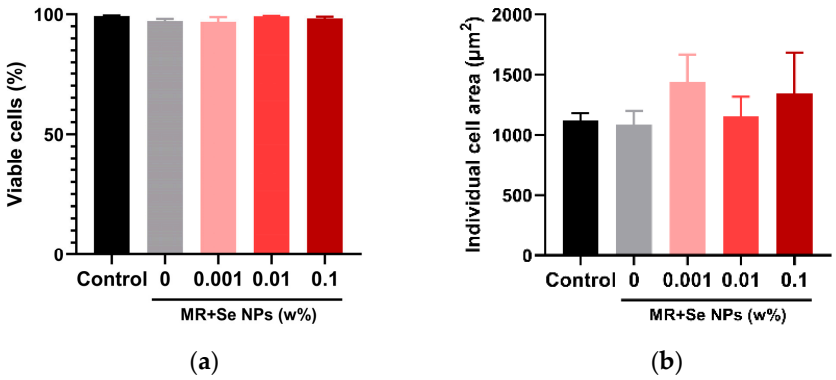
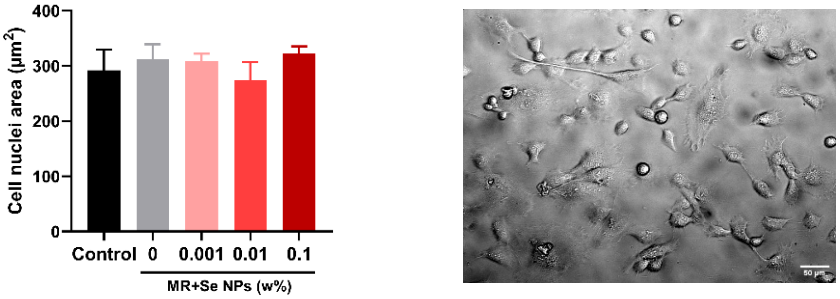


Figure 13. *Cont.*



(**c**) (**d**)

Figure 13. Results of cytotoxicity assessment of samples printed from MR and Se NPs-MR. Average values of viability (**a**), individual cell areas (**b**), and cell nuclei (**c**) after 72 h of cultivation. Image of cells in transmitted light, cultured with samples of materials printed from Se NPs-MR containing 0.1 w% Se NPs (**d**).

3. Discussion

Currently, modified photopolymerizable resins based on methacrylate monomers have gained widespread popularity for additive manufacturing of finished products. A notable example of such products is self-disinfecting materials and surfaces, which utilize NPs with antibacterial properties as a functional component to impede the proliferation of bacterial cells. A compelling and extensively deliberated illustration of this phenomenon is Se NPs, which have demonstrated remarkable antibacterial efficacy against a diverse array of microorganisms [33–36]. The choice of Se NPs as a modifying agent is due not only to their effective antibacterial action, but also to their high degree of biocompatibility.

Se NPs were synthesized by pulsed laser ablation in an aqueous solution [37]. The liquid pulse laser ablation method is one of the most promising approaches for the synthesis of inorganic NPs, serving as a reliable alternative to traditional chemical methods [38]. The key advantages of this technology are the elimination of toxic reagents (acids, alkalis) and the absence of chemical contamination of the synthesized NPs. According to the literature, laser ablation can be used to obtain NPs with a controlled size in the range of 5–120 nm with adjustable colloidal and functional properties [39]. The dynamic light scattering method revealed a monomodal distribution of NPs with a peak at 75 nm and a half-width of approximately 50 nm (Figure 1a). The study of the distribution of the electrokinetic potential of Se NPs showed a monomodal character with a pronounced maximum at -35 mV (Figure 1b), which indicates the high stability of the obtained colloidal solution of NPs. Analysis of the optical properties of the colloid revealed moderate absorption in the visible region of the spectrum (380–750 nm), characteristic of amorphous selenium (Se^0) NPs, with a characteristic absorption peak in the region of 260–265 nm (Figure 1c). Morphological study of Se NPs using transmission electron microscopy showed that the particles are spherical in shape with an average size of about 70 nm (Figure 1d). The obtained aqueous colloids of Se NPs were redispersed in acetone and transferred into a methacrylate photopolymer resin, from which samples of plates used for further studies were successfully printed. These composite samples were easily sanded and polished (Figure 2a). To verify the accuracy of the modified resins, a volumetric sample with a regular mesh structure and a pore size of about 500 μm was also printed (Figure 2b). The results obtained indicate that the incorporation of Se NPs does not affect the accuracy of the original methacrylate resin, which may be of interest for the additive manufacturing of products with complex geometry and high accuracy [40]. When transferring Se NPs from an aqueous colloidal system to a photopolymer resin, some increase in the surface roughness of the printed samples was observed, which is probably due to partial aggregation of NPs on the surface of the printed samples. Unlike the control samples (Figure 3a), composites

printed from Se NPs-MR showed an increase in average roughness values with maximum height differences in the range of 60–80 nm (Figure 3b). Previous data suggest that the observed changes in topographical characteristics indicate effective dispersion of selenium NPs in the polymer matrix and their influence on surface formation processes in additive manufacturing [41]. It is important to note that despite increased roughness, the composite plate samples obtained retained high surface quality without the formation of microscopic defects, pores, or cracks, which often occur in additive manufacturing from heterogeneous substrates. The occurrence of structural defects, in particular induced porosity, in the additive manufacturing process has a significant impact on the performance characteristics and functional reliability of products made from polymer composites [42]. An important characteristic of the surfaces of multicomponent materials is their hydrophobic–hydrophilic properties. It was found that the initial polymer matrix is characterized by moderately hydrophilic properties, which is typical of many photopolymerizable resins containing polar functional groups in their structure (Figure 4a–d). The observed tendency to decrease the contact angle with an increase in the concentration of Se NPs, despite the lack of statistical significance in this study, is of significant interest from the point of view of modification of surface properties (Figure 4e). The discovered hydrophilizing effect can be explained by several interrelated mechanisms. Firstly, the incorporation of Se NPs is capable of leading to a change in the surface energy of the composite due to an increase in surface roughness and the creation of additional wetting centers [43]. Secondly, the presence of inorganic NPs in the polymer matrix can cause a redistribution of the polar functional groups of the resin at the phase boundary, which contributes to an increase in the hydrophilic nature of the surface [44]. In addition, the influence of the intrinsic surface properties of selenium, which in a nanodispersed state can exhibit increased chemical activity [45], cannot be ruled out.

Studies conducted on the distribution of Se NPs in the polymer matrix confirmed the absence of defects in the form of voids in the samples. It was found that Se NPs are unevenly distributed in the polymer matrix, forming areas with varying concentrations, which can be visualized using a modulation interference microscope as alternating zones with increased and decreased nanoparticle distribution density (Figure 5a–d). A number of studies have shown that clustering and partial aggregation of NPs during the modification of photopolymers can occur prior to the polymerization process and can be caused by the precipitation of NPs and subsequent agglomeration of particles in the lower layers of the printed part [46]. In a recent paper, Gil et al. considered adding a dispersion emulsifier to the photopolymer in the resin as a solution to this problem, allowing the NPs to remain suspended in the mixture for a long time [47].

Another common problem with MSLA printing is the incomplete conversion of monomers in the volume of the polymer product obtained using additive technology. It is known that residual monomers remaining in the polymer matrix after photopolymerization can migrate to the surface of the material, leading to a significant reduction in the mechanical properties and chemical stability of the resulting products [48,49]. The toxicological aspect poses a particular danger—leaching of unreacted monomers can induce cytotoxic effects, limiting the use of such materials in medical implants and devices [50,51]. The low conversion rate of monomers also causes post-polymerization, leading to uncontrolled changes in the geometry of products during operation [52]. As a result, it is necessary to achieve the maximum level of monomer conversion to ensure the proper physical properties of the finished products and their satisfactory biocompatibility [53]. For example, the critical level of photoconversion for medical devices is 95–98% [54]. The conversion rate of monomers in photopolymer materials is increased through a combination of technological and chemical-physical approaches, including: optimization of photopolymer-

ization parameters by controlling the intensity of UV radiation, its spectral composition, and exposure time; modification of the resin composition by introducing highly reactive monomers with reduced viscosity; the use of cross-linking agents that reduce segmental mobility and prevent radical recombination; thermal post-treatment of printed products; the development of hybrid photoinitiator systems with controlled kinetic behavior and the use of additives that absorb residual monomers [55,56]. The polymerization of methacrylates proceeds through the breaking of the π-bond in the vinyl group (C=C) of the methacrylic fragment, which initiates the formation of active centers and the subsequent attachment of monomer units with the formation of a polymer chain [57]. This process refers to chain radical reactions and is characterized by the formation of σ-bonds between monomers [58]. To study the degree of polymerization of the obtained composite samples using IR Fourier transform absorption spectrometry, the intensity of peaks in the range 1600–1650 cm^{-1}, corresponding to C=C bond vibrations, was evaluated. The incorporation of the initial Se NPs resin in a low concentration (0.001 w%) led to an increase in the intensity of absorption in this wavelength range, while an increase in concentration to 0.1 w% led to a decrease in intensity, which indicated an increase in the degree of photopolymerization of methacrylate monomers (Figure 6a). It is likely that the incorporation of Se NPs into the methacrylate resin at higher concentrations contributes to the intensification of the photopolymerization process, leading to a decrease in the proportion of residual monomers. This effect may be due to the ability of Se NPs to act as photoactive centers, increasing the quantum yield of photopolymerization through additional absorption and scattering of radiation, as well as potential catalytic effects [59]. The results obtained for optical absorption in the visible and UV regions of the composite samples demonstrated no change in the optical characteristics of the materials (Figure 6b).

Assessment of the influence of composites obtained from modified resins on the processes of generating active oxygen species (H_2O_2 and ·OH) in aqueous media demonstrated an increase in the formation of the studied ROS upon contact with samples made from an unmodified polymer matrix. Incorporation of Se NPs photopolymer resin at concentrations of 0.01 and 0.1 w%, on the contrary, led to a significant decrease in the concentrations of all studied active oxygen species (Figure 7a,b). The formation of ROS can either stimulate [60] or inhibit a number of biological processes [61]. For example, high concentrations of ROS in biological systems cause oxidative stress, accompanied by oxidative damage to biomolecules such as DNA and proteins [62]. At the same time, the addition of antioxidants can significantly reduce the degree of damage to such biomolecules [63,64]. In in vitro experiments, we demonstrated the ability of composites containing Se NPs to inhibit the formation of LRPS and 8-oxoguanines in DNA, which are indicators of oxidative damage to protein molecules and DNA, respectively (Figure 8a,b). 8-oxoguanine is one of the most significant biomarkers of oxidative DNA damage, formed as a result of the reaction of guanine with reactive oxygen species, in particular hydroxyl radicals [65]. This modification leads to base pairing disruption, causing G→T transversions and mutation accumulation, which are associated with carcinogenesis [66] and aging [67] processes. The observed effects may be due to the catalytic activity of Se NPs in the decomposition of peroxide compounds and the neutralization of free radicals [68–70]. The direct antioxidant activity of Se NPs is well described in the literature [12,71]. It has been reported that Se NPs are capable of exhibiting peroxidase-like activity, accelerating the reduction of H_2O_2 to water molecules with simultaneous oxidation of selenium to hydroselenous acid (H_2SeO_3) [72,73]. In turn, Se NPs effectively neutralize ·OH radicals through direct electron transfer, forming stable selenium compounds [74].

When evaluating the antibacterial properties of the composites obtained, we used a comprehensive approach, including both studying the effect of materials on the kinetics

of bacterial growth using photometric measurement of the optical density of the bacterial suspension and applying a precision method of flow cytometry using differential staining with propidium iodide. Analysis of daily growth curves showed a slight decrease in the optical density of bacterial suspensions when cultured with pure polymer samples; at the same time, a significant inhibition of *E. coli* suspension growth by ~75–85% was observed when using composites containing all the Se NPs concentrations considered (Figure 9). When performing cytometric measurements of bacterial suspensions, a significant increase in the proportion of dead bacterial cells (up to ~20%) was observed only for composites containing 0.1w% Se NPs (Figures 10 and 11a). At the same time, quantitative counting of *E. coli* cells in the suspension showed a decrease in the content of bacterial units in all groups of material samples containing Se NPs (Figure 11b). The result obtained was comparable to the results of the evaluation of *E. coli* growth curves and indicated the pronounced bacteriostatic properties of the obtained composite samples, but not bactericidal properties. The observed antibacterial effect of materials obtained from resins incorporating Se NPs can be explained by several factors simultaneously. Firstly, unlike metal NPs and metal oxide NPs (ZnO, TiO_2, CuO), Se NPs do not cause such severe destabilization of lipid membranes or destruction of the peptidoglycan layer [75,76]. In particular, acrylic composites with Se NPs have been reported to destroy the cell walls of microorganisms only at concentrations of 10% and above [75]. In addition, Se NPs are capable of activating bacterial antioxidant defense systems, which allows them to neutralize the products of free radical reactions formed when exposed to NPs; this compensatory mechanism prevents the bactericidal effect from occurring [77–79]. To evaluate cytocompatibility, the effect of composites on the growth of human HSF cells was investigated. Microscopic analysis revealed minor morphological changes in isolated cells during prolonged cultivation in the presence of composite samples (Figure 12a–f). However, quantitative assessment of viability by double staining (Hoechst 33342/PI) confirmed the preservation of a high proportion of viable cells in all experimental groups without statistically significant differences from the control (Figure 13a–d). The results obtained are consistent with other studies demonstrating good cytocompatibility of Se NP-containing polymeric materials [80,81]. In particular, the work of Saleem et al. demonstrated the effectiveness of the combined use of Se NPs in photopolymerizable dental resins, similar to our results; the inclusion of a 1% mixture of Se and ZnO NPs contributed to higher biocompatibility of the material compared to the separate use of ZnO NPs, against the background of significant antibacterial properties of the materials under consideration [82]. Our results confirm the promise of using the modified photopolymerizable bases we have developed in areas where a combination of antimicrobial properties and high cytocompatibility of the resulting products is required.

4. Materials and Methods

4.1. Synthesis of Se NPs Colloid and Production of Se NPs-MR

Se NPs were synthesized by laser ablation of a high-purity (99.99%) target in deionized water [83]. The volume of the liquid was 100 mL; the specific electrical conductivity was 0.1 μS/cm. An Nd:YAG laser generating radiation with a wavelength (λ) of 532 nm, a pulse frequency of 1 kHz, a pulse duration (τ) of 4 ns, and an energy of 1.5 mJ was used for the synthesis. The characteristics of the obtained NPs, including size, zeta potential, and concentration, were determined using a Malvern Zetasizer Ultra analyzer (Malvern Panalytical Ltd., Malvern, UK). The optical properties of the colloid were studied by UV-visible spectroscopy using a CINTRA 4040 (GBC Scientific Equipment Pty Ltd., Keysborough, Australia). The morphology of Se NPs was investigated using a Libra 200 FE HR transmission electron microscope (Carl Zeiss, Oberkochen, Germany).

To prepare modified MR (Se NPs-MR), Se NPs were first transferred from an aqueous dispersion to acetone. This process involved centrifuging the initial dispersion, removing the supernatant, and adding fresh acetone to the nanoparticle precipitate, followed by ultrasonic treatment and vortex shaking. The centrifugation and solvent replacement procedure were repeated three times to completely replace the medium. The resulting Se NPs dispersion in acetone was mixed with methacrylic resin until final nanoparticle concentrations of 0.001%, 0.01%, and 0.1% by weight were achieved. The initial MR is a transparent liquid with a viscosity of 1000 ± 200 mPa·s, compliant with ISO 10993 [84] and registered under certificate RZN 2020/12007. To ensure uniform distribution of NPs in the resin, mechanical mixing on a shaker and ultrasonic treatment (40 kHz, 22 °C, 5 min) were performed. To store the finished Se NPs-MR materials, sealed dark glass containers were used, which were placed in conditions excluding exposure to light.

4.2. Additive Manufacturing from Modified Resins

Samples of the obtained Se NPs-MR composites were manufactured using an additive method on a Saturn 3 Ultra 12K MSLA printer (Elegoo, Shenzhen, China). Before printing, a pre-prepared modified MR was poured into the printer's vat. A control group of samples was made from pure MR without NPs. For each material composition, round plates with a diameter of 16 mm and a thickness of 0.5 mm were printed for physicochemical and biological studies, as well as volumetric samples with a mesh architecture. All printed samples underwent a multi-step post-processing process. First, they were rinsed in absolute isopropanol on a magnetic stirrer for 6 min, then ultrasonically cleaned in isopropanol for 6 min. Afterwards, the samples were dried at room temperature for 10 min and then subjected to finishing treatment, which involved applying glycerin and subsequent UV curing on a rotating platform for 30 min (UW-02, Creality3D, Shenzhen, China). The ultrasonic treatment and drying process was then repeated. The final step was thermal annealing in an oven at 80 °C for 30 min. The prepared samples were stored under standard laboratory conditions, placing them in closed Petri dishes.

4.3. Physical and Chemical Characteristics of Composites Obtained from Se NPs-MR

The micro- and nanostructure of the surface of samples printed from Se NPs-MR was studied using a morphology analysis complex manufactured by NT-MDT (NT-MDT LLC, Zelenograd, Russia) with semi-contact measurement modes. The hydrophilic-hydrophobic characteristics of the synthesized composite materials' surfaces were studied using the static contact angle (sessile drop) method. Measurements were performed on a contact angle analyzer under standard laboratory conditions (temperature 23 ± 2 °C, relative humidity 50 ± 5%). A volume of 3 μL of distilled water was applied to the pre-ground and degreased surfaces of the sample plates using an automatic dispenser. The shape of the resulting droplet was recorded using a CMOS camera SDU3-C264 (SpetsTeleTechnika, Moscow, Russia). For each sample, at least ten independent measurements were performed at different points on the surface. The contact angle (θc) was calculated automatically using the DropSnake and LB-ADSA macros for ImageJ software 1.54g. The interaction of NPs with the polymer matrix was studied using an IR-8000 FTIR spectrometer (SAS LLC, Krasnoyarsk, Russia) equipped with a ZnSe Sealed Flat Plate attachment (Pike Technologies, Fitchburg, WI, USA), as well as a dual-beam UV/Vis spectrometer Cintra 4040 (GBC Scientific Equipment Pty Ltd., Victoria, Australia). The analysis of the distribution of Se NPs in the polymer matrix was performed using a modulation interference microscope MIM-321 (Amphora laboratories, Moscow, Russia).

4.4. Quantitative Assessment of Reactive Oxygen Species (ROS) Formation in Aqueous Solutions (·OH and H_2O_2)

Using highly sensitive analytical approaches, the formation of reactive oxygen species in aqueous solutions after their incubation with printed Se NPs-MR composites was quantified, including the determination of hydrogen peroxide (H_2O_2) and hydroxyl radical (·OH) content. The concentration of hydrogen peroxide was determined by chemiluminescence using a highly sensitive Biotox-7A-USE chemiluminometer (ANO "Engineering Center—Ecology," Moscow, Russia). Measurements were performed in a reaction system containing luminol, 4-iodophenol, and horseradish peroxidase in Tris-HCl buffer (pH 8.5) [85]. Composite samples in the form of 10 × 10 × 0.5 mm plates were placed in polypropylene vials (Beckman, CA, USA) with distilled water and incubated at 40 °C for 3 h. Then, a freshly prepared counting solution containing 1 mM Tris-HCl buffer, 50 μM para-iodophenol, 50 μM luminol, and 10 nM horseradish peroxidase (pH 8.5) was added. This technique is extremely sensitive and allows the detection of hydrogen peroxide at concentrations below 0.1 nM. Comparisons with known antioxidants as positive controls were not per-formed because the efficacy of Se NPs is significantly inferior to known strong antioxidants.

For quantitative determination of hydroxyl radicals, a fluorimetric method based on the reaction with coumarin-3-carboxylic acid (CCA) was used [86]. Thin film samples (⌀16 mm, thickness 0.5 mm) were placed in vials containing CCA solution in phosphate-saline buffer and incubated at 80.0 ± 0.1 °C for 2 h. A spectrofluorimetric study of a series of composite samples containing 0.001–0.1 wt.% Se NPs was performed on a JASCO 8300 instrument (JASCO, Tokyo, Japan), recording the reaction product—7-hydroxycoumarin-3-carboxylic acid—at excitation wavelengths of 400 nm and emission wavelengths of 450 nm. All experiments, performed in triplicate to ensure statistical reliability, were accompanied by control measurements without samples to account for background signals.4.5. Quantitative determination of 8-oxoguanine in DNA and long-lived reactive protein species (LRPS)

Quantitative determination of 8-oxoguanine content in DNA samples was performed by enzyme-linked immunosorbent assay using specific monoclonal antibodies [87]. Sample preparation began with bringing DNA samples to a concentration of 350 μg/mL, followed by denaturation by heating in a water bath for 5 min and rapid cooling on ice. For analysis, 42 μL of prepared DNA was added to the wells of the plate, where the molecules were immobilized at 80 °C for 3 h. Non-specific binding sites were blocked with a 1% solution of skimmed milk in Tris-HCl buffer (pH 8.7) with the addition of 0.15 M NaCl for 14–18 h at room temperature. In the next step, primary antibodies to 8-oxoguanine, diluted 1:2000, were added to the wells and incubated at 37 °C for 3 h. After washing, secondary antibodies conjugated with horseradish peroxidase (dilution 1:1000) were added, followed by incubation at 37 °C for 1.5 h. The enzymatic reaction was detected using ABTS substrate (18.2 mM) in the presence of 2.6 mM H_2O_2 in 75 mM citrate buffer (pH 4.2). The reaction was stopped by adding 100 μL of 1.5 mM sodium azide when discoloration appeared. Optical density was measured at a wavelength of 405 nm on a Feyond-A400 plate reader (Allsheng, Hangzhou, China).

The change in the concentration of LRPS was assessed using the chemiluminescence method [88]. This method is effective and sensitive for determining free radical reactions. The Biotox-7A-USE chemiluminometer (ANO "Engineering Center—Ecology," Moscow, Russia) was used to study LRPS by measuring the chemiluminescence of bovine serum albumin protein solutions at elevated temperatures. Chemiluminescence measurements were performed in the dark at room temperature in 20 mL polypropylene plastic vials (Beckman, CA, USA). The samples were preheated in a water bath to 45 °C for 2 h. Unheated protein solutions were used as controls. Comparisons with known antioxidants as positive

controls were not per-formed because the efficacy of Se NPs is significantly inferior to known strong antioxidants.

4.5. Microbiological Assay

Before studying the antibacterial properties of the printed Se NPs-MR composites, the samples were prepared: they were placed in the wells of a 24-well plate, treated with 70% C_2H_5OH (ethanol alcohol) solution (1 mL/well), and sterilized with UV radiation in a laminar flow hood for 40 min. At the same time, an *Escherichia coli* bacterial suspension was prepared: a colony of bacteria was transferred with a sterile loop to 10 mL of sterile LB broth and cultured in a shaker incubator at 37 °C and 230 rpm overnight [89]. Before the experiment, the overnight culture was diluted 1000 times with fresh broth to a concentration of approximately 10^6 CFU/mL and thoroughly mixed on a vortex mixer. After adding 1000 μL of bacterial suspension to each well with the test material, the open plate was placed in a Feyond-A400 plate photometer (Allsheng, Hangzhou, China) with a thermostat and shaking system. For 24 h at a constant temperature of 37 °C and with periodic shaking, automated measurements of the optical density of bacterial cultures at 600 nm were performed hourly. Based on the data obtained, growth curves were constructed, analyzing the effect of materials on the duration of the lag phase, the rate of exponential growth, and the maximum density of bacterial cultures. Pure polymer without Se NPs and sterile broth without bacteria were used as controls. Comparisons with known antibiotics as positive controls were not performed because the efficacy of Se NPs is significantly inferior to known strong antibiotics.

For additional microbiological analysis, flow cytometry was used [90]. Sample preparation and bacterial cultivation in the presence of composite materials were per-formed in accordance with the above-described method. After cultivation, 1 mL of phosphate-buffered saline containing 4 μM PI (Lumiprobe, Westminster, MD, USA) was added to each sample. When bound to DNA, this dye emits an orange-red glow with an absorption maximum at 535 nm and an emission maximum at 617 nm, and the quantum yield of the complex with DNA is 20–30 times higher than that of the free dye. The plate with the added dye was incubated in the dark for 60 min, after which the samples were resuspended and transferred to clean tubes for subsequent analysis on a Longcyte cytometer (Challenbio, Beijing, China).

4.6. In Vitro Cytotoxicity Assay

The cytotoxicity of the printed composites was investigated on human spleen fibroblast (HSF) cells (#5530, ScienCell, Carlsbad, CA, USA) obtained from ScienCell. The cells were cultured under standard conditions in DMEM/F12 medium supplemented with 2 mM L-glutamine, 10% FBS, and streptomycin (25 μg/mL) with penicillin (25 IU/mL) (all from PanEco, Moscow, Russia). Before starting the experiment, Ø25 mm round cover glasses were sterilized at 180 °C for 2 h. A cell suspension with a density of 10^5 cells in 200 μL of medium was applied to the prepared slides and placed in the wells of a 6-well plate. To ensure cell adhesion, the plate was incubated for 30 min in an S-Bt Smart Biotherm CO_2 incubator (Biosan, Riga, Latvia) at 37 °C and 5% CO_2. Then, 1800 μL of fresh nutrient medium was added to each well and the composite material samples under study were placed in the wells. Cultivation continued for 72 h under controlled conditions. After incubation, samples were removed, and the cell cultures were analyzed microscopically. A combination of fluorescent dyes was used to assess cell viability: Hoechst 33342 for staining nuclei, rhodamine for visualizing mitochondria, and propidium iodide for detecting dead cells (all from Lumiprobe, Westminster, MD, USA). Cellular imaging and recording were performed using a DMI 4000B system (Leica, Wetzlar, Germany).

4.7. Statistical Processing and Data Visualization

Experimental data processing and statistical analysis were performed using GraphPad Prism software version 8.3.0. Analysis of micrographs of cell cultures was performed using ImageJ software version 2.14.0. All results are presented as mean values with standard error of the mean. To obtain reliable data, the results of at least three independent experiments were used.

5. Conclusions

Consequently, the developed photopolymerizable composites based on methacrylate resins modified with Se NPs, synthesized by pulsed laser ablation, exhibit a set of functional properties that determine their potential for creating self-disinfecting materials for additive manufacturing. In the course of our work, we demonstrated the successful integration of Se NPs into a polymer matrix while preserving both the physicochemical and biological properties characteristic of these NPs. The printed composite samples exhibited the following characteristics: the absence of structural defects, a controlled increase in surface roughness, moderate aggregation of NPs, and moderate wettability. A salient feature of the obtained materials is their dual functionality, which manifests as both pronounced antioxidant activity and a bacteriostatic effect. It has been demonstrated that composites containing 0.01–0.1 w% Se NPs effectively suppress the generation of active oxygen species (H_2O_2 and ·OH) in aqueous media, which correlates with a decrease in the formation of biomarkers of oxidative damage (8-oxoguanine in DNA and LRPS). Concurrently, evidence was presented that demonstrated a dose-dependent inhibition of *E. coli* growth, exhibiting a 75–85% reduction in bacterial density while maintaining high mammalian cell viability (HSF line). This outcome serves to confirm the selectivity of antimicrobial action. The developed composites hold particular pertinence for biomedical applications, encompassing the fabrication of bespoke implants and medical devices that necessitate a synthesis of additive manufacturing precision, functional activity, and biocompatibility.

Author Contributions: Conceptualization, S.V.G.; methodology, A.V.S.; software, M.E.A.; formal analysis, A.V.S.; investigation, D.E.B., I.V.B., F.M.Y., V.A.K. and D.A.S.; writing—original draft preparation, D.E.B.; writing—review and editing, S.V.G.; visualization, D.E.B. and F.M.Y.; supervision, S.V.G.; project administration, F.M.Y. All authors have read and agreed to the published version of the manuscript.

Funding: This research was funded by a grant from the Ministry of Science and Higher Education of the Russian Federation, grant number 075-15-2024-646.

Institutional Review Board Statement: Not applicable.

Informed Consent Statement: Not applicable.

Data Availability Statement: The raw data supporting the conclusions of this article will be made available by the authors upon request.

Acknowledgments: The authors thank the Center for Collective Use of the GPI RAS.

Conflicts of Interest: The authors declare no conflicts of interest.

Abbreviations

The following abbreviations are used in this manuscript:

AFM	Atomic Force Microscopy
ROS	Reactive Oxygen Species
LRPS	Long-lived Reactive Protein Species
OD	Optical Density

PI	Propidium Iodide
Se NPs	Selenium nanoparticles
MR	Methacrylate Resin

References

1. Li, Y.; Jiang, D.; Zhu, R.; Yang, C.; Wang, L.; Zhang, L.-C. Revolutionizing medical implant fabrication: Advances in additive manufacturing of biomedical metals. *Int. J. Extrem. Manuf.* **2024**, *7*, 022002. [CrossRef]
2. Lu, Y.; Xu, W.; Leng, J.; Liu, X.; Xu, H.; Ding, H.; Zhou, J.; Cui, L. Review and Research Prospects on Additive Manufacturing Technology for Agricultural Manufacturing. *Agriculture* **2024**, *14*, 1207. [CrossRef]
3. Ng, W.L.; Goh, G.L.; Goh, G.D.; Ten, J.S.J.; Yeong, W.Y. Progress and Opportunities for Machine Learning in Materials and Processes of Additive Manufacturing. *Adv. Mater.* **2024**, *36*, e2310006. [CrossRef]
4. Zafar, M.S. Prosthodontic Applications of Polymethyl Methacrylate (PMMA): An Update. *Polymers* **2020**, *12*, 2299. [CrossRef] [PubMed]
5. Sabri, B.A.; Satgunam, M.; Abreeza, N.; Abed, A.N.; Jones, I.P. A review on enhancements of PMMA Denture Base Material with Different Nano-Fillers. *Cogent Eng.* **2021**, *8*, 1875968. [CrossRef]
6. Guo, R.; Kan, Y.-C.; Xu, Y.; Han, L.-Y.; Bu, W.-H.; Han, L.-X.; Qi, Y.-Y.; Chu, J.-J. Preparation and efficacy of antibacterial methacrylate monomer-based polymethyl methacrylate bone cement containing N-halamine compounds. *Front. Bioeng. Biotechnol.* **2024**, *12*, 1414005. [CrossRef]
7. Zore, A.; Abram, A.; Učakar, A.; Godina, I.; Rojko, F.; Štukelj, R.; Škapin, A.S.; Vidrih, R.; Dolic, O.; Veselinovic, V.; et al. Antibacterial Effect of Polymethyl Methacrylate Resin Base Containing TiO2 Nanoparticles. *Coatings* **2022**, *12*, 1757. [CrossRef]
8. Gudkov, S.V.; Sarimov, R.M.; Astashev, M.E.; Pishchalnikov, R.Y.; Yanykin, D.V.; Simakin, A.V.; Shkirin, A.V.; Serov, D.A.; Konchekov, E.M.; Namik Guseynagaogly, G.-Z.; et al. Modern physical methods and technologies in agriculture. *Phys. Uspekhi* **2023**, *67*, 194–210. [CrossRef]
9. Selmani, A.; Kovačević, D.; Bohinc, K. Nanoparticles: From synthesis to applications and beyond. *Adv. Colloid Interface Sci.* **2022**, *303*, 102640. [CrossRef]
10. Bano, I.; Skalickova, S.; Sajjad, H.; Skladanka, J.; Horky, P. Uses of Selenium Nanoparticles in the Plant Production. *Agronomy* **2021**, *11*, 2229. [CrossRef]
11. Varlamova, E.G.; Turovsky, E.A.; Blinova, E.V. Therapeutic Potential and Main Methods of Obtaining Selenium Nanoparticles. *Int. J. Mol. Sci.* **2021**, *22*, 10808. [CrossRef]
12. Dawood, M.A.O.; Basuini, M.F.E.; Yilmaz, S.; Abdel-Latif, H.M.R.; Kari, Z.A.; Abdul Razab, M.K.A.; Ahmed, H.A.; Alagawany, M.; Gewaily, M.S. Selenium Nanoparticles as a Natural Antioxidant and Metabolic Regulator in Aquaculture: A Review. *Antioxidants* **2021**, *10*, 1364. [CrossRef]
13. Geoffrion, L.D.; Hesabizadeh, T.; Medina-Cruz, D.; Kusper, M.; Taylor, P.; Vernet-Crua, A.; Chen, J.; Ajo, A.; Webster, T.J.; Guisbiers, G. Naked Selenium Nanoparticles for Antibacterial and Anticancer Treatments. *ACS Omega* **2020**, *5*, 2660–2669. [CrossRef]
14. Behera, A.; Dharmalingam Jothinathan, M.K.; Saravanan, S.; Tamil Selvan, S.; Rajan Renuka, R.; Srinivasan, G.P. Green Synthesis of Selenium Nanoparticles From Clove and Their Toxicity Effect and Anti-angiogenic, Antibacterial and Antioxidant Potential. *Cureus* **2024**, *16*, e55605. [CrossRef]
15. Ansari, J.A.; Malik, J.A.; Ahmed, S.; Manzoor, M.; Ahemad, N.; Anwar, S. Recent advances in the therapeutic applications of selenium nanoparticles. *Mol. Biol. Rep.* **2024**, *51*, 688. [CrossRef]
16. Bisht, N.; Phalswal, P.; Khanna, P.K. Selenium nanoparticles: A review on synthesis and biomedical applications. *Mater. Adv.* **2022**, *3*, 1415–1431. [CrossRef]
17. Ferro, C.; Florindo, H.F.; Santos, H.A. Selenium Nanoparticles for Biomedical Applications: From Development and Characterization to Therapeutics. *Adv. Healthc. Mater.* **2021**, *10*, 2100598. [CrossRef] [PubMed]
18. Shahidin; Wang, Y.; Wu, Y.; Chen, T.; Wu, X.; Yuan, W.; Zhu, Q.; Wang, X.; Zi, C. Selenium and Selenoproteins: Mechanisms, Health Functions, and Emerging Applications. *Molecules* **2025**, *30*, 437. [CrossRef]
19. Yuan, S.; Zhang, Y.; Dong, P.-Y.; Chen Yan, Y.-M.; Liu, J.; Zhang, B.-Q.; Chen, M.-M.; Zhang, S.-E.; Zhang, X.-F. A comprehensive review on potential role of selenium, selenoproteins and selenium nanoparticles in male fertility. *Heliyon* **2024**, *10*, e34975. [CrossRef]
20. Varlamova, E.G. Roles of selenium-containing glutathione peroxidases and thioredoxin reductases in the regulation of processes associated with glioblastoma progression. *Arch. Biochem. Biophys.* **2025**, *766*, 110344. [CrossRef] [PubMed]
21. Zoidis, E.; Seremelis, I.; Kontopoulos, N.; Danezis, G. Selenium-Dependent Antioxidant Enzymes: Actions and Properties of Selenoproteins. *Antioxidants* **2018**, *7*, 66. [CrossRef] [PubMed]
22. Nastulyavichus, A.; Kudryashov, S.; Smirnov, N.; Saraeva, I.; Rudenko, A.; Tolordava, E.; Ionin, A.; Romanova, Y.; Zayarny, D. Antibacterial coatings of Se and Si nanoparticles. *Appl. Surf. Sci.* **2019**, *469*, 220–225. [CrossRef]

23. Belenichev, I.F.; Gorchakova, N.O.; Bukhtiyarova, N.V.; Samura, I.B.; Savchenko, N.V.; Popazova, O.O. Pharmacological properties of selenium and its preparations: From antioxidant to neuroprotector. *Res. Results Pharmacol.* **2021**, *7*, 29–40. [CrossRef]
24. Burmistrov, D.E.; Shumeyko, S.A.; Semenova, N.A.; Dorokhov, A.S.; Gudkov, S.V. Selenium Nanoparticles (Se NPs) as Agents for Agriculture Crops with Multiple Activity: A Review. *Agronomy* **2025**, *15*, 1591. [CrossRef]
25. Chaudhary, S.; Mehta, S.K. Selenium Nanomaterials: Applications in Electronics, Catalysis and Sensors. *J. Nanosci. Nanotechnol.* **2014**, *14*, 1658–1674. [CrossRef]
26. ElSheikh, S.K.; Eid, E.-S.G.; Abdelghany, A.M.; Abdelaziz, D. Physical/mechanical and antibacterial properties of composite resin modified with selenium nanoparticles. *BMC Oral Health* **2024**, *24*, 1245. [CrossRef]
27. Abdelnour, S.A.; Alagawany, M.; Hashem, N.M.; Farag, M.R.; Alghamdi, E.S.; Hassan, F.U.; Bilal, R.M.; Elnesr, S.S.; Dawood, M.A.O.; Nagadi, S.A.; et al. Nanominerals: Fabrication Methods, Benefits and Hazards, and Their Applications in Ruminants with Special Reference to Selenium and Zinc Nanoparticles. *Animals* **2021**, *11*, 1916. [CrossRef]
28. Tsivileva, O.; Pozdnyakov, A.; Ivanova, A. Polymer Nanocomposites of Selenium Biofabricated Using Fungi. *Molecules* **2021**, *26*, 3657. [CrossRef]
29. Xia, J.; Li, T.; Lu, C.; Xu, H. Selenium-Containing Polymers: Perspectives toward Diverse Applications in Both Adaptive and Biomedical Materials. *Macromolecules* **2018**, *51*, 7435–7455. [CrossRef]
30. Sowmya, R.; Karthick Raja Namasivayam, S.; Krithika Shree, S. A Critical Review on Nano-selenium Based Materials: Synthesis, Biomedicine Applications and Biocompatibility Assessment. *J. Inorg. Organomet. Polym. Mater.* **2024**, *34*, 3037–3055. [CrossRef]
31. Sarosi, C.; Moldovan, M.; Soanca, A.; Roman, A.; Gherman, T.; Trifoi, A.; Chisnoiu, A.M.; Cuc, S.; Filip, M.; Gheorghe, G.F.; et al. Effects of Monomer Composition of Urethane Methacrylate Based Resins on the C=C Degree of Conversion, Residual Monomer Content and Mechanical Properties. *Polymers* **2021**, *13*, 4415. [CrossRef]
32. Rudenko, Y.; Kozlov, V.; Burmistrov, D.; Fedyakova, N.; Bermeshev, M.; Chapala, P. Comprehensive investigation of phosphine oxide photoinitiators for vat photopolymerization. *Prog. Addit. Manuf.* **2025**, *10*, 8405–8418. [CrossRef]
33. Yuan, Q.; Xiao, R.; Afolabi, M.; Bomma, M.; Xiao, Z. Evaluation of Antibacterial Activity of Selenium Nanoparticles against Food-Borne Pathogens. *Microorganisms* **2023**, *11*, 1519. [CrossRef]
34. Ionin, A.A.; Ivanova, A.K.; Khmel'nitskii, R.A.; Klevkov, Y.V.; Kudryashov, S.I.; Levchenko, A.O.; Nastulyavichus, A.A.; Rudenko, A.A.; Saraeva, I.N.; Smirnov, N.A.; et al. Antibacterial effect of the laser-generated Se nanocoatings on Staphylococcus aureus and Pseudomonas aeruginosa biofilms. *Laser Phys. Lett.* **2018**, *15*, 015604. [CrossRef]
35. Perfileva, A.I.; Moty'leva, S.M.; Klimenkov, I.V.; Arsent'ev, K.Y.; Graskova, I.A.; Sukhov, B.G.; Trofimov, B.A. Development of Antimicrobial Nano-Selenium Biocomposite for Protecting Potatoes from Bacterial Phytopathogens. *Nanotechnologies Russ.* **2018**, *12*, 553–558. [CrossRef]
36. Saraeva, I.N.; Tolordava, E.R.; Khmelnitsky, R.A.; Shelygina, S.N.; Pozdnyakova, D.S.; Nastulyavichus, A.A.; Rimskaya, E.N.; Rupasov, A.E. Effect of Selenium, Copper and Silver Microparticles Obtained in Viscous Media on the Gram-Positive and Gram-Negative Bacteria Survival. *JETP Lett.* **2025**, *121*, 306–314. [CrossRef]
37. Baimler, I.V.; Simakin, A.V.; Dorokhov, A.S.; Gudkov, S.V. Mini-review on laser-induced nanoparticle heating and melting. *Front. Chem.* **2024**, *12*, 1463612. [CrossRef] [PubMed]
38. Quintana, M.; Haro-Poniatowski, E.; Morales, J.; Batina, N. Synthesis of selenium nanoparticles by pulsed laser ablation. *Appl. Surf. Sci.* **2002**, *195*, 175–186. [CrossRef]
39. Fahad, O.A.; Abdulkareem, F.A.; Mohammed, A.S.; Kareem, O.A. Produce of Selenium Nanoparticles by Pulsed Laser Ablation for Anticancer Treatments. *Int. J. Nanosci.* **2022**, *20*, 2150055. [CrossRef]
40. Colorado, H.A.; Gutierrez-Velasquez, E.I.; Gil, L.D.; de Camargo, I.L. Exploring the advantages and applications of nanocomposites produced via vat photopolymerization in additive manufacturing: A review. *Adv. Compos. Hybrid Mater.* **2023**, *7*, 1. [CrossRef]
41. Rahman, M.M.; Khan, K.H.; Parvez, M.M.H.; Irizarry, N.; Uddin, M.N. Polymer Nanocomposites with Optimized Nanoparticle Dispersion and Enhanced Functionalities for Industrial Applications. *Processes* **2025**, *13*, 994. [CrossRef]
42. Folorunso, O.; Hamam, Y.; Sadiku, R.; Kupolati, W. Effects of Defects on the Properties of Polymer Nanocomposites: A Brief Review. *J. Inorg. Organomet. Polym. Mater.* **2024**, *34*, 5667–5690. [CrossRef]
43. Manoudis, P.N.; Karapanagiotis, I. Modification of the wettability of polymer surfaces using nanoparticles. *Prog. Org. Coat.* **2014**, *77*, 331–338. [CrossRef]
44. Majumder, A.; Radzanowski, A.N.; Wang, C.-Y.; Mu, Y.; Coughlin, E.B.; Gorte, R.J.; Vohs, J.M.; Lee, D. Modulating the Contact Angle between Nonpolar Polymers and SiO2 Nanoparticles. *Macromolecules* **2024**, *57*, 8554–8561. [CrossRef]
45. Wang, J.; Li, J.; Xie, L.; Shi, C.; Liu, Q.; Zeng, H. Interactions between elemental selenium and hydrophilic/hydrophobic surfaces: Direct force measurements using AFM. *Chem. Eng. J.* **2016**, *303*, 646–654. [CrossRef]
46. Shah, M.; Ullah, A.; Azher, K.; Rehman, A.U.; Juan, W.; Aktürk, N.; Tüfekci, C.S.; Salamci, M.U. Vat photopolymerization-based 3D printing of polymer nanocomposites: Current trends and applications. *RSC Adv.* **2023**, *13*, 1456–1496. [CrossRef]

47. Gil, L.D.; Monteiro, S.N.; Colorado, H.A. Polymer Matrix Nanocomposites Fabricated with Copper Nanoparticles and Photopolymer Resin via Vat Photopolymerization Additive Manufacturing. *Polymers* **2024**, *16*, 2434. [CrossRef]
48. Wu, J.; Zhao, Z.; Hamel, C.M.; Mu, X.; Kuang, X.; Guo, Z.; Qi, H.J. Evolution of material properties during free radical photopolymerization. *J. Mech. Phys. Solids* **2018**, *112*, 25–49. [CrossRef]
49. Lang, M.; Hirner, S.; Wiesbrock, F.; Fuchs, P. A Review on Modeling Cure Kinetics and Mechanisms of Photopolymerization. *Polymers* **2022**, *14*, 2074. [CrossRef]
50. Zhang, Y.; Paul, T.; Brehm, J.; Völkl, M.; Jérôme, V.; Freitag, R.; Laforsch, C.; Greiner, A. Role of Residual Monomers in the Manifestation of (Cyto)toxicity by Polystyrene Microplastic Model Particles. *Environ. Sci. Technol.* **2023**, *57*, 9925–9933. [CrossRef]
51. Kostić, M.; Stanojević, J.; Tačić, A.; Gligorijević, N.; Nikolić, L.; Nikolić, V.; Igić, M.; Bradić Vasić, M. Determination of residual monomer content in dental acrylic polymers and effect after tissues implantation. *Biotechnol. Biotechnol. Equip.* **2020**, *34*, 254–263. [CrossRef]
52. Truffier-Boutry, D.; Demoustier-Champagne, S.; Devaux, J.; Biebuyck, J.-J.; Mestdagh, M.; Larbanois, P.; Leloup, G. A physico-chemical explanation of the post-polymerization shrinkage in dental resins. *Dent. Mater.* **2006**, *22*, 405–412. [CrossRef]
53. Arif, U.; Haider, S.; Haider, A.; Khan, N.; Alghyamah, A.A.; Jamila, N.; Khan, M.I.; Almasry, W.A.; Kang, I.-K. Biocompatible Polymers and their Potential Biomedical Applications: A Review. *Curr. Pharm. Des.* **2019**, *25*, 3608–3619. [CrossRef]
54. Kaufmann, B.K.; Rudolph, M.; Pechtl, M.; Wildenburg, G.; Hayden, O.; Clausen-Schaumann, H.; Sudhop, S. mSLAb—An open-source masked stereolithography (mSLA) bioprinter. *HardwareX* **2024**, *19*, e00543. [CrossRef]
55. Ajay, R.; Suma, K.; Ali, S. Monomer modifications of denture base acrylic resin: A systematic review and meta-analysis. *J. Pharm. Bioallied Sci.* **2019**, *11*, S112–S125. [CrossRef]
56. Ceylan, G.; Emik, S.; Yalcinyuva, T.; Sunbuloğlu, E.; Bozdag, E.; Unalan, F. The Effects of Cross-Linking Agents on the Mechanical Properties of Poly (Methyl Methacrylate) Resin. *Polymers* **2023**, *15*, 2387. [CrossRef]
57. Edo, G.I.; Ndudi, W.; Ali, A.B.M.; Yousif, E.; Zainulabdeen, K.; Onyibe, P.N.; Akpoghelie, P.O.; Ekokotu, H.A.; Isoje, E.F.; Igbuku, U.A.; et al. An updated review on the modifications, recycling, polymerization, and applications of polymethyl methacrylate (PMMA). *J. Mater. Sci.* **2024**, *59*, 20496–20539. [CrossRef]
58. Molina-Gutiérrez, S.; Dalle Vacche, S.; Vitale, A.; Ladmiral, V.; Caillol, S.; Bongiovanni, R.; Lacroix-Desmazes, P. Photoinduced Polymerization of Eugenol-Derived Methacrylates. *Molecules* **2020**, *25*, 3444. [CrossRef] [PubMed]
59. Chen, M.; Zhong, M.; Johnson, J.A. Light-Controlled Radical Polymerization: Mechanisms, Methods, and Applications. *Chem. Rev.* **2016**, *116*, 10167–10211. [CrossRef] [PubMed]
60. Belov, S.V.; Danyleiko, Y.K.; Glinushkin, A.P.; Kalinitchenko, V.P.; Egorov, A.V.; Sidorov, V.A.; Konchekov, E.M.; Gudkov, S.V.; Dorokhov, A.S.; Lobachevsky, Y.P.; et al. An Activated Potassium Phosphate Fertilizer Solution for Stimulating the Growth of Agricultural Plants. *Front. Phys.* **2021**, *8*, 616. [CrossRef]
61. Gudkov, S.V.; Gudkova, O.Y.; Chernikov, A.V.; Bruskov, V.I. Protection of mice against X-ray injuries by the post-irradiation administration of guanosine and inosine. *Int. J. Radiat. Biol.* **2009**, *85*, 116–125. [CrossRef] [PubMed]
62. Karmanova, E.E.; Goncharov, R.G.; Bruskov, V.I.; Novoselov, V.I.; Sharapov, M.G. The Radioprotective Effect of Exogenous Peroxiredoxin 6 in Mice Exposed to Different Doses of Whole-Body Ionizing Radiation. *Biophysics* **2025**, *69*, 1153–1160. [CrossRef]
63. Lankin, V.Z.; Shumaev, K.B.; Medvedeva, V.A.; Tikhaze, A.K.; Konovalova, G.G. Mechanisms of Antioxidant Protection of Low-Density Lipoprotein Particles Against Free Radical Oxidation. *Biochemistry* **2025**, *90*, 107–119. [CrossRef]
64. Baranova, E.N.; Kononenko, N.V.; Lapshin, P.V.; Nechaeva, T.L.; Khaliluev, M.R.; Zagoskina, N.V.; Smirnova, E.A.; Yuorieva, N.O.; Raldugina, G.N.; Chaban, I.A.; et al. Superoxide Dismutase Premodulates Oxidative Stress in Plastids for Protection of Tobacco Plants from Cold Damage Ultrastructure Damage. *Int. J. Mol. Sci.* **2024**, *25*, 5544. [CrossRef] [PubMed]
65. Dzhimak, S.; Baryshev, M.; Malyshko, V.; Dorohova, A.; Il'chenko, G.; Tekutskaya, E. 8-Oxoguanine-DNA-Glycosylase Gene Polymorphism and the Effects of an Alternating Magnetic Field on the Sensitivity of Peripheral Blood. *Front. Biosci. Landmark* **2023**, *28*, 252. [CrossRef]
66. Viel, A.; Bruselles, A.; Meccia, E.; Fornasarig, M.; Quaia, M.; Canzonieri, V.; Policicchio, E.; Urso, E.D.; Agostini, M.; Genuardi, M.; et al. A Specific Mutational Signature Associated with DNA 8-Oxoguanine Persistence in MUTYH-defective Colorectal Cancer. *EBioMedicine* **2017**, *20*, 39–49. [CrossRef]
67. Li, L.; Zhang, X. The Significance of 8-oxoGsn in Aging-Related Diseases. *Aging Dis.* **2020**, *11*, 1329–1338. [CrossRef]
68. Sentkowska, A.; Pyrzyńska, K. Antioxidant Properties of Selenium Nanoparticles Synthesized Using Tea and Herb Water Extracts. *Appl. Sci.* **2023**, *13*, 1071. [CrossRef]
69. Xu, X.; Pan, Y.; Liu, X.; Han, Z.; Chen, S. Constructing Selenium Nanoparticles with Enhanced Storage Stability and Antioxidant Activities via Conformational Transition of Curdlan. *Foods* **2023**, *12*, 563. [CrossRef]
70. Sentkowska, A.; Pyrzyńska, K. The Influence of Synthesis Conditions on the Antioxidant Activity of Selenium Nanoparticles. *Molecules* **2022**, *27*, 2486. [CrossRef]
71. Gudkov, S.V.; Gao, M.; Simakin, A.V.; Baryshev, A.S.; Pobedonostsev, R.V.; Baimler, I.V.; Rebezov, M.B.; Sarimov, R.M.; Astashev, M.E.; Dikovskaya, A.O.; et al. Laser Ablation-Generated Crystalline Selenium Nanoparticles Prevent Damage of DNA and

Proteins Induced by Reactive Oxygen Species and Protect Mice against Injuries Caused by Radiation-Induced Oxidative Stress. *Materials* **2023**, *16*, 5164. [CrossRef]
72. Chen, X.; Zhu, X.; Gong, Y.; Yuan, G.; Cen, J.; Lie, Q.; Hou, Y.; Ye, G.; Liu, S.; Liu, J. Porous selenium nanozymes targeted scavenging ROS synchronize therapy local inflammation and sepsis injury. *Appl. Mater. Today* **2021**, *22*, 100929. [CrossRef]
73. Dumore, N.S.; Mukhopadhyay, M. Antioxidant properties of aqueous selenium nanoparticles (ASeNPs) and its catalysts activity for 1, 1-diphenyl-2-picrylhydrazyl (DPPH) reduction. *J. Mol. Struct.* **2020**, *1205*, 127637. [CrossRef]
74. Muñoz Barbosa, M.T.; Mejía Diaz, L.F.; Wrobel, K.; Corrales Escobosa, A.R.; Miranda-Aviles, R.; Wrobel, K. Selenium Nanoparticles Act as Hydrogen Peroxide Scavengers in a Simulated Biological Environment. *ChemistrySelect* **2025**, *10*, e202500433. [CrossRef]
75. Rostamzadeh, M.; Sadeghi Sangdehi, S.A.; Salimizand, H.; Rahimi, F.; Nouri, B. Evaluating the anti-Candida effects of selenium nanoparticles impregnated in acrylic resins: An in vitro study. *J. Dent. Res. Dent. Clin. Dent. Prospect.* **2024**, *18*, 258–263. [CrossRef] [PubMed]
76. Huang, X.; Chen, X.; Chen, Q.; Yu, Q.; Sun, D.; Liu, J. Investigation of functional selenium nanoparticles as potent antimicrobial agents against superbugs. *Acta Biomater.* **2016**, *30*, 397–407. [CrossRef]
77. Cameron, S.J.; Sheng, J.; Hosseinian, F.; Willmore, W.G. Nanoparticle Effects on Stress Response Pathways and Nanoparticle–Protein Interactions. *Int. J. Mol. Sci.* **2022**, *23*, 7962. [CrossRef]
78. Webster, T.; Wang, Q.; Larese-Casanova, P. Inhibition of various gram-positive and gram-negative bacteria growth on selenium nanoparticle coated paper towels. *Int. J. Nanomed.* **2015**, *2015*, 2885–2894. [CrossRef]
79. Cremonini, E.; Zonaro, E.; Donini, M.; Lampis, S.; Boaretti, M.; Dusi, S.; Melotti, P.; Lleo, M.M.; Vallini, G. Biogenic selenium nanoparticles: Characterization, antimicrobial activity and effects on human dendritic cells and fibroblasts. *Microb. Biotechnol.* **2016**, *9*, 758–771. [CrossRef]
80. Abdelhamid, A.E.; Ahmed, E.H.; Awad, H.M.; Ayoub, M.M.H. Synthesis and cytotoxic activities of selenium nanoparticles incorporated nano-chitosan. *Polym. Bull.* **2023**, *81*, 1421–1437. [CrossRef]
81. Ji, H.; Lou, X.; Jiao, J.; Li, Y.; Dai, K.; Jia, X. Preliminary Structural Characterization of Selenium Nanoparticle Composites Modified by Astragalus Polysaccharide and the Cytotoxicity Mechanism on Liver Cancer Cells. *Molecules* **2023**, *28*, 1561. [CrossRef] [PubMed]
82. Saleem, I.; Rana, N.F.; Tanweer, T.; Arif, W.; Shafique, I.; Alotaibi, A.S.; Almukhlifi, H.A.; Alshareef, S.A.; Menaa, F. Effectiveness of Se/ZnO NPs in Enhancing the Antibacterial Activity of Resin-Based Dental Composites. *Materials* **2022**, *15*, 7827. [CrossRef]
83. Gorudko, I.V.; Grigorieva, D.V.; Gusakov, G.A.; Baran, L.V.; Reut, V.E.; Sak, E.V.; Baimler, I.V.; Simakin, A.V.; Dorokhov, A.S.; Izmailov, A.Y.; et al. Rod and spherical selenium nanoparticles: Physicochemical properties and effects on red blood cells and neutrophils. *Biochim. Biophys. Acta (BBA)—Gen. Subj.* **2025**, *1869*, 130777. [CrossRef]
84. *ISO 10993-1:2018*; Biological Evaluation of Medical Devices. ISO: Geneva, Switzerland, 2018.
85. Sevostyanov, M.A.; Kolmakov, A.G.; Sergiyenko, K.V.; Kaplan, M.A.; Baikin, A.S.; Gudkov, S.V. Mechanical, physical–chemical and biological properties of the new Ti–30Nb–13Ta–5Zr alloy. *J. Mater. Sci.* **2020**, *55*, 14516–14529. [CrossRef]
86. Baimler, I.V.; Gudkov, S.V.; Matveeva, T.A.; Simakin, A.V.; Shcherbakov, I.A. Generation of Reactive Oxygen Species during Water Drops Fall on a Solid Surface. *Phys. Wave Phenom.* **2024**, *32*, 187–189. [CrossRef]
87. Chernikov, A.V.; Gudkov, S.V.; Shtarkman, I.N.; Bruskov, V.I. Oxygen effect in heat-induced DNA damage. *Biofizika* **2007**, *52*, 244–251. [CrossRef]
88. Gudkov, S.V.; Shtarkman, I.N.; Chernikov, A.V.; Usacheva, A.M.; Bruskov, V.I. Guanosine and inosine (riboxin) eliminate the long-lived protein radicals induced X-ray radiation. *Dokl. Biochem. Biophys.* **2007**, *413*, 50–53. [CrossRef] [PubMed]
89. Burmistrov, D.E.; Simakin, A.V.; Smirnova, V.V.; Uvarov, O.V.; Ivashkin, P.I.; Kucherov, R.N.; Ivanov, V.E.; Bruskov, V.I.; Sevostyanov, M.A.; Baikin, A.S.; et al. Bacteriostatic and Cytotoxic Properties of Composite Material Based on ZnO Nanoparticles in PLGA Obtained by Low Temperature Method. *Polymers* **2021**, *14*, 49. [CrossRef]
90. Burmistrov, D.E.; Serov, D.A.; Baimler, I.V.; Gritsaeva, A.V.; Chapala, P.; Simakin, A.V.; Astashev, M.E.; Karmanova, E.E.; Dubinin, M.V.; Nizameeva, G.R.; et al. Polymethyl Methacrylate-like Photopolymer Resin with Titanium Metal Nanoparticles Is a Promising Material for Biomedical Applications. *Polymers* **2025**, *17*, 1830. [CrossRef] [PubMed]

Disclaimer/Publisher's Note: The statements, opinions and data contained in all publications are solely those of the individual author(s) and contributor(s) and not of MDPI and/or the editor(s). MDPI and/or the editor(s) disclaim responsibility for any injury to people or property resulting from any ideas, methods, instructions or products referred to in the content.